Published in "Physical Review B - Condensed Matter and
Materials Physics 86(14): 144112, 2012"
which should be cited to refer to this work.

Far-infrared spectra of the magnetic exchange resonances and optical phonons and their connection to magnetic and dielectric properties of $Dy_3Fe_5O_{12}$ garnet

T. D. Kang,* E. C. Standard, P. D. Rogers, K. H. Ahn, and A. A. Sirenko
Department of Physics, New Jersey Institute of Technology, Newark, New Jersey 07102, USA

A. Dubroka and C. Bernhard
Department of Physics, University of Fribourg, CH-1700 Fribourg, Switzerland

S. Park
Rutgers Center for Emergent Materials and Department of Physics and Astronomy, Rutgers University, Piscataway, New Jersey 08854, USA and Department of Physics, Chung-Ang University, Seoul 156-756, Korea

Y. J. Choi
Rutgers Center for Emergent Materials and Department of Physics and Astronomy, Rutgers University, Piscataway, New Jersey 08854, USA and Department of Physics and IPAP, Yonsei University, Seoul 120-749, Korea

S.-W. Cheong
Rutgers Center for Emergent Materials and Department of Physics and Astronomy, Rutgers University, Piscataway, New Jersey 08854, USA

Far-infrared spectra of ferrimagnetic $Dy_3Fe_5O_{12}$ single crystals have been studied in the spectral range between 12 and 700 cm^{-1} and in a wide temperature range between 5 K and 300 K using transmission spectroscopy and rotating analyzer ellipsometry. In the temperature range below $T_C = 16$ K for the magnetic ordering of Dy^{3+} spins, a number of ligand field and Kaplan-Kittel (KK) exchange resonance modes have been found. Temperature dependencies of their frequencies allowed us to estimate the ratio between the Fe-Dy and Dy-Dy exchange constants. We found that variation of the oscillator strength of the KK modes correlates with the magnetic-field-induced changes of magnetic permeability. The low-temperature peak in the static value of the dielectric function at $T_C = 16$ K may be related to the observed temperature-induced variation of the oscillator strength of the optical phonons.

I. INTRODUCTION

Magneto-optical effects, the ferrimagnetic structure of the Fe spin sublattice, and its relationship to the huge magnetostriction in rare earth iron garnets (R-IGs), with the chemical formula $R_3Fe_5O_{12}$ (R = Tb, Dy, Ho, Er, etc.), have been in the research focus for decades.[1] An interest in R-IGs was renewed after the recent discovery of the magnetoelectric and magnetodielectric effects in Tb-IG in surprisingly low magnetic fields of less than 2 kOe.[2] Formation of the local electric polarization induced by the magnetic ordering was also observed in Tb-IG.[3] These reports were followed by far-IR spectroscopic studies of the coupling between magnons and ligand-field excitations in Tb-IG in the temperature range of ~70 K.[4] These results bring up a number of new questions about the interconnection between the crystal and magnetic structure with the far-IR optical excitations in the related R-IG compounds, such as Dy-IGs.

Tb and Dy are neighbors in the line of R^{3+} ions and are different by one f electron only. But the electron parity change in the $4f$ orbital and different spin and g-factor values between Tb and Dy may result in a significant modification of the low-temperature magnetic and dielectric properties between Dy-IG and Tb-IG. Recently we presented preliminary results for antiferroelectric (AFE) ordering in Dy-IG that occurs in the same temperature range ($T < 16$ K) as the ferromagnetic (FM) ordering of Dy^{3+} spins.[5] The latter has not been observed in Tb-IG yet, probably due to a significantly lower transition temperature. A magnetodielectric effect revealed itself in Dy-IG at low temperatures as a relatively small increase of the static dielectric constant in a weak magnetic field of ~1 kOe (0.1 T).[5] Our particular interest in R-IGs follows the mainstream of modern studies of magnetoelectric and multiferroic materials.[6–10] The microscopic nature of the magnetoelectric effects can be better understood through studies of optical excitations such as IR-active electromagnons and lattice vibrations that are modified by the spin-lattice interaction.[11–19] Due to the coincidence of the temperatures for the FM ordering of Dy spins and the AFE lattice ordering in Dy-IG, we expected an interesting behavior for the low-frequency optical phonons, which are related to the displacements of the heaviest ions (Dy) and spin-related ligand field (LF) transitions and Kaplan-Kittel (KK)[20] magnetic exchange resonance modes in Dy-IG. The main results of this paper are (i) the observed correlation between the magnetic-field-induced changes of magnetic susceptibility $\chi(0,H)$ with the oscillator strength of the KK modes and (ii) the established Lyddane-Sachs-Teller (LST) relation between the static dielectric constant $\varepsilon(0,T)$ and the oscillator strength of the low-frequency optical phonons in proximity to the AFE phase transition. We will also show that the peak in $\varepsilon(0,H)$ at ~1 kOe is not related to the spectra of the LF and KK modes suggesting that the magnetodielectric effect

is probably driven by the magnetic-field-induced changes in the spectra of the optical phonons.

This paper is organized as follows. The structural and magnetic properties of Dy-IG known from the literature are summarized in Sec. II. Details of experimental techniques for far-IR transmission spectroscopy and spectroscopic ellipsometry are presented in Sec. III. The original results of this paper are shown in Secs. IV–VI. Temperature dependencies of the far-IR-active excitations measured in the proximity of the FM phase transition for Dy spins at $T_C = 16$ K is presented in Sec. IV. A short overview of the literature for the far-IR excitations in Dy-IG is followed by the discussion of the experimental data. The LF and KK modes are identified and the temperature dependence of their frequencies is shown to be related to magnetization due to Dy spins. Spectra of the LF, crystal field (CF), and KK excitations measured in external magnetic field are presented in Sec. V. Effective g factors for the CF and LF transitions are determined. Special attention is given to the variation of the LF and KK mode oscillator strength in weak magnetic fields because the magnetodielectric effect in Dy-IG has been previously reported for $H \leqslant 10$ kOe.[5] In Sec. VI we discuss optical phonon spectra obtained with spectroscopic ellipsometry.

II. MATERIAL AND MAGNETIC PROPERTIES OF Dy-IG

Dy-IG, as well as the other related R-IGs, is a ferrimagnetic material with huge magnetostriction, which is related to the combination of a strong anisotropy of the crystal field of the R^{3+} ions and to a strong and anisotropic superexchange interaction between R^{3+} and iron.[21–23] At room temperature $Dy_3Fe_5O_{12}$ crystals form a cubic structure with a space group $Ia3d(O_h^{10})$. The figures of the crystal and magnetic structure of R-IGs can be found, for example, in Refs. 22 and 23. Dy^{3+} ions with the ground state $^6H_{15/2}$ are in the 24d dodecahedral sites with the local orthorhombic symmetry $222(D_2)$. There are several nonequivalent Dy^{3+} ions in each unit cell with the same surrounding field, but the axes are inclined to each other. This has the overall effect of producing an average cubic symmetry. Fe^{3+} ions occupy two sites: 16a octahedral sites with the $\bar{3}(C_{3i})$ symmetry and 24c tetrahedral sites with the $\bar{4}(S_4)$ symmetry. Below the transition temperature of $T_N \approx 550$ K, the iron spins are ordered in a ferrimagnetic structure along the [111] direction. Among six possible exchange interactions between spins in three different magnetic subsystems (a, c, and d) only two dominate.[21,22] The main magnetic superexchange interaction is between Fe in two different sites (a and c): Spins of Fe in the tetrahedral site are antiparallel to those of the octahedral site. Another important interaction is between Dy and Fe in the tetrahedral site resulting in the Dy spins to be antiparallel to Fe moments in the tetrahedral sites, and, hence, antiparallel to the net magnetic moment of Fe. At $T_{com} = 223$ K the total magnetization of Dy and Fe sublattices is compensated: $M = 0$. The temperature dependence of $\chi(T) = M(T)/H$ from Ref. 5 is shown in Fig. 1(a) where the compensation point at $T_{com} = 223$ K is marked with an arrow. Below 100 K, a rhombohedral distortion of the cubic cell causes the canting of Dy spins, which is described as a "double umbrella structure."[24] The symmetry of Dy^{3+} is lowered from $222(D_2)$ tetragonal to $2(C_2)$ monoclinic. Below

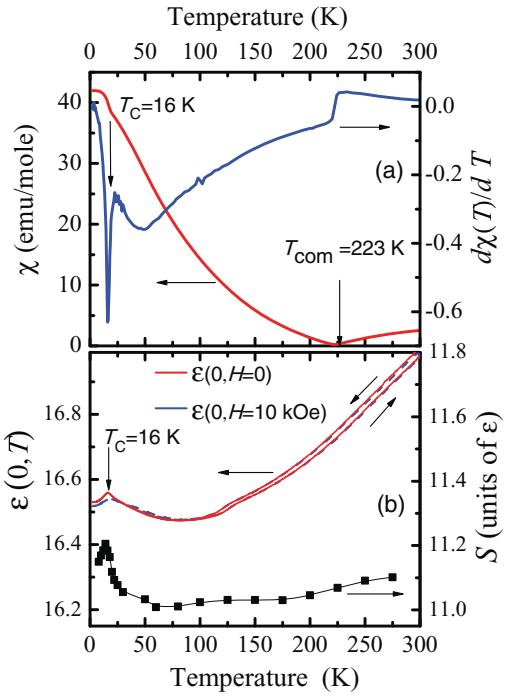

FIG. 1. (Color online) (a) Temperature dependence of the static magnetic susceptibility (red curve) and its derivative (blue curve) for $Dy_3Fe_5O_{12}$ single crystal from Ref. 5. FM ordering of Dy^{3+} spins occurs at $T_C = 16$ K. The compensation point for the total Fe and Dy magnetization is marked with a vertical arrow at $T_{com} = 223$ K. (b) Temperature dependence of the static dielectric constant at $H = 0$ (red) and at $H = 10$ kOe (blue) from Ref. 5. The total oscillator strength $\sum_j^N S_j(T)$ of all optical phonons measured using spectroscopic ellipsometry is shown with black squares. Note that the right and left vertical scales in (b) have an offset of 5.2, which is close to ε_∞ for Dy-IG.

50 K, the iron sublattice magnetization does not change appreciably with temperature. However, the Dy sublattice magnetization increases rapidly with the temperature decrease. It is reflected in the change of $\partial\chi(T)/\partial T$ for $T < 50$ K in Fig. 1(a). The anomaly in $\partial\chi(T)/\partial T$ at $T_C = 16$ K corresponds to the appearance of the FM ordering for Dy^{3+} spins.[5] This transition was also studied by specific-heat and high-field-magnetization measurements and was associated with the iron spin reorientation from the easy ⟨111⟩ axis to a low-symmetry angular phase.[25,26] A slightly lower transition temperature of 14.5 K was reported in Ref. 25.

III. SAMPLES AND MEASUREMENTS

The high-temperature flux growth technique was utilized to produce bulk crystals of $Dy_3Fe_5O_{12}$. Our recent experimental data from Ref. 5 for the static magnetic susceptibility $\chi(0,T)$ and dielectric constant $\varepsilon(0,T)$ are shown in Figs. 1(a) and 1(b). The dielectric constant $\varepsilon(0,T)$ was measured at a single frequency of 44 kHz for a sample with the (011) plane. Other samples from the same batch with the (001) and (111) planes, a cross-section area of 5×5 mm^2, and different thicknesses of 0.19 and 0.50 mm were used for the optical experiments: transmission and rotating analyzer ellipsometry (RAE). The opposite sides of the sample were polished and

wedged with a ∼3° offset in order to suppress interference fringes. Transmission spectra were measured with a resolution of 0.3 cm^{-1} in the spectral range between 13 and 100 cm^{-1} at the National Synchrotron Light Source, Brookhaven National Laboratory, at the U4IR beamline equipped with a Bruker IR spectrometer and a LHe-pumped (∼1.4 K) bolometer. A magnetic field of up to 100 kOe (10 T) was applied to the sample along the light propagation direction (Faraday configuration). Polarization of the transmitted light was not analyzed. For each sample the raw data of transmitted intensity were normalized to transmission through an empty aperture with the size equal to that of the sample. The RAE measurements of the optical phonons were carried out at Fribourg University. The RAE experimental setup is similar to that described in Ref. 27. A conventional Hg lamp was used as a light source. Spectra of optical phonons in Dy-IG have been measured in the temperature range between 8 and 300 K in the spectral range between 70 and 690 cm^{-1} and resolution of 0.7 cm^{-1} using a single value for the angle of incidence (AOI) of 75°. Additional RAE measurements of the same sample have been carried out at room temperature in the energy range between 0.75 eV and 5.9 eV using the J. A. Woollam spectroscopic ellipsometer at the Center for Functional Nanomaterials, Brookhaven National Laboratory.

IV. FAR-IR EXCITATIONS IN *R*-IG

Far-IR spectra of magnetic excitations in *R*-IG (*R* = Sm, Gd, Ho, Er, and Yb) were studied more than 40 years ago by Sievers and Tinkham.[28,29] Yamomoto *et al*. studied far-IR spectra for Dy-IG and Tb-IG.[30] It appeared that Dy-IG had the most complex spectrum of the far-IR excitations among all other studied *R*-IGs. Based on the analysis of transmission in polycrystalline materials it was shown that below 80 cm^{-1} the optical spectra of *R*-IGs are dominated by both R^{3+} single-ion electronic transitions and KK modes. Note that in all earlier studies of the far-IR excitations in *R*-IG it was assumed that the optical transitions inside the $4f$ shell are magnetic dipoles, as expected for a free R^{3+} ion or for an R^{3+} ion at the center of inversion.[20,28–30,]

Synchrotron radiation spectroscopy allows data collection in a broader range of external parameters, such as external magnetic fields and low temperatures. As we will see in this section, the advanced spectroscopic capabilities enable observation of effects that were not detectable in the earlier experiments with polycrystalline *R*-IG samples carried out with a lower spectral resolution. Recent studies of *R*-IG show that at low temperatures the local electric polarization removes the R^{3+} ions from the position at the center of inversion.[3,5] This result is important for interpretation of the selection rules for the optical transitions between the $4f$ electronic levels of Dy^{3+}. In the noncentrosymmetric environment, the so-called "forced electric dipole" optical transitions are allowed in addition to the conventional magnetic-dipole transitions.[31] In our recent study of the far-IR excitations in Tb-IG we observed a coupling between magnons and ligand field electronic excitations of Tb^{3+} and suggested that the tuning of the dielectric constant by temperature and magnetic field can be connected to the appearance of the hybrid magnetoelectric modes.[4] In contrast, in the present studies of Dy-IG we found a stronger connection between the static dielectric constant and the spectra of the optical phonons (see Sec. VI of this paper). Also, we recently reported an observation of hybridization between electric- and magnetic-dipole activity for the ligand-field excitations, which was only possible due to the combined analysis of the transmission, reflection, and RAE spectra of Dy-IG.[5] In this paper we will rely on the previously determined type of the dipole activity for the LF and KK modes from Ref. 5 and will focus on the temperature and magnetic field changes of the frequency and oscillator strength for the LF and KK modes in connection with the changes of the static dielectric constant $\varepsilon(0,T,H)$ and magnetic susceptibility $\chi(0,T,H)$.

Figures 2(a)–2(e) show far-IR ellipsometry data for the real part of a pseudodielectric function $\langle\varepsilon_1\rangle$ at $T = 8$ K and several transmittivity spectra measured at $T = 5$, 19, and 35 K for the Dy-IG sample with the thickness $d = 0.50$ mm. The major oscillator modes in $\langle\varepsilon_1\rangle$ and absorption minima, which correspond to the IR-active modes, are marked with arrows in Figs. 2(a)–2(e). Several spectral modes in the frequency range between 70 and 100 cm^{-1} [see in Figs. 2(b)–2(e)] are saturated due to strong absorption in a relatively thick sample with $d = 0.50$ mm. To improve our sensitivity to the position of the saturated peaks, we polished the same Dy-IG sample down to the thickness of $d = 0.19$ mm and repeated the transmission measurements. The corresponding transmission intensity spectra Tr.(T) for $T = 4$ K and $T = 300$ K are shown in Fig. 3(a). All modes that were saturated in Fig. 2(b) can be clearly seen in Fig. 3(a). The high-temperature spectra Tr.(T) measured for $T > 200$ K have only one absorption mode that corresponds to lowest frequency optical phonon at 80 cm^{-1}. The contribution of this optical phonon to the room temperature spectrum Tr.(300 K) corresponds to the signal below the blue dashed line in Fig. 3(a). The room temperature spectrum without the optical phonon contribution was used for normalization of the transmission intensity measured at low temperatures in Figs. 3(b) and 4(b). The corresponding spectra of Tr.(T)/Tr.(300 K) measured at $T = 4$, 12, 18, and 23 K are shown in Fig. 3(b). The absorption peaks are marked with arrows. To illustrate the temperature-induced evolution of the transmittivity spectra of the thick sample ($d = 0.50$ mm) and that for the normalized transmission spectra of the thin sample ($d = 0.19$ mm) we present the two-dimensional (2D) intensity maps in Figs. 4(a) and 4(b), which were measured with the temperature increments of 1 K. Positions of all absorption peaks measured with both ellipsometry and transmission techniques are summarized in Fig. 4(c).

The lowest frequency IR-active optical phonon at 81 cm^{-1} is visible in the whole measured temperature range in both ellipsometry [Fig. 2(a)] and transmittivity spectra [Figs. 2(b)–2(e)], and in normalized transmission spectra [Figs. 3(a) and 3(b)]. Its properties along with that for all other optical phonons will be discussed in Sec. VI. For relatively high temperatures $T \geqslant 20$ K, only a few single-ion crystal-field (CF) electronic transitions of Dy^{3+} at about 20, 53, 63, 71 (doublet), and 87 cm^{-1} can be seen in Figs. 4(a) and 4(b), where the corresponding absorption lines are marked as CF1, CF2, CF3, CF4, and CF5. The nearly temperature-independent frequencies of these lines are typical for CF transitions. Similar

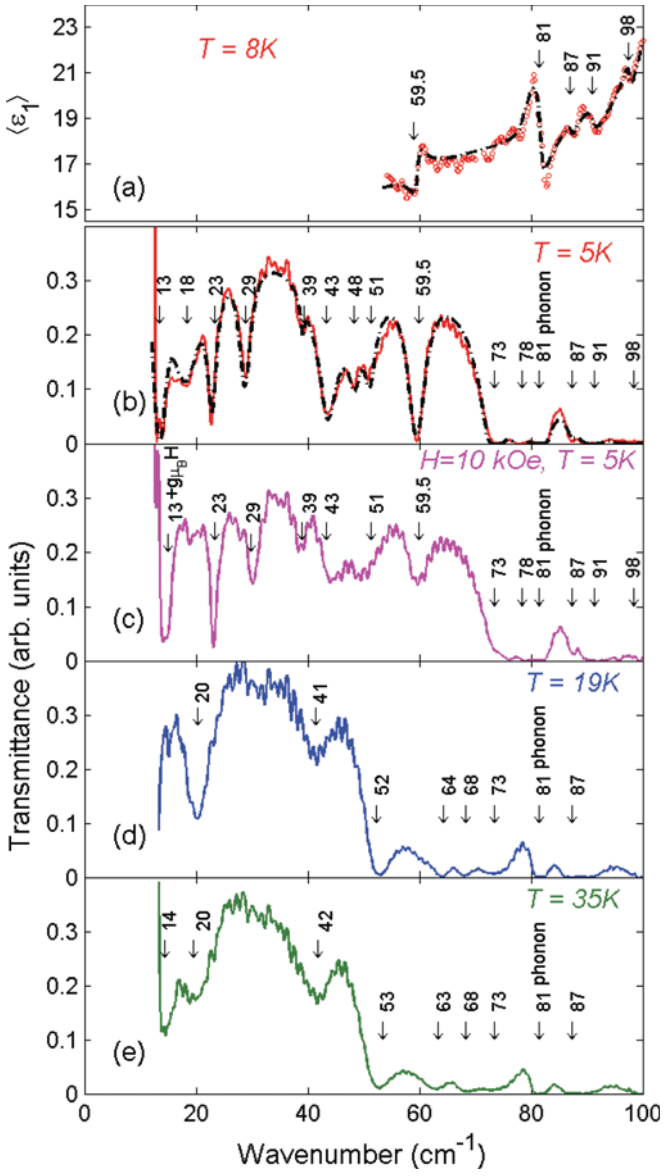

FIG. 2. (Color online) (a) Far-IR ellipsometry spectrum for the real part of the pseudodielectric function for $Dy_3Fe_5O_{12}$ single crystal that is dominated by the optical phonon at 81 cm^{-1}, a magnetic dipole excitation at 59.5 cm-1, and three hybrid modes at 87, 91, and 98 cm^{-1}. (b) Far-IR transmission spectra for the same sample with the thickness of $d = 0.50$ mm measured in a zero external magnetic field at $T = 5$ K, (c) $T = 5$ K and $H = 10$ kOe, (d) zero field and $T = 19$ K, and (e) 35 K. The light propagation for transmission spectra is along the [100] direction. Arrows indicate the frequencies of the IR-active absorption lines.

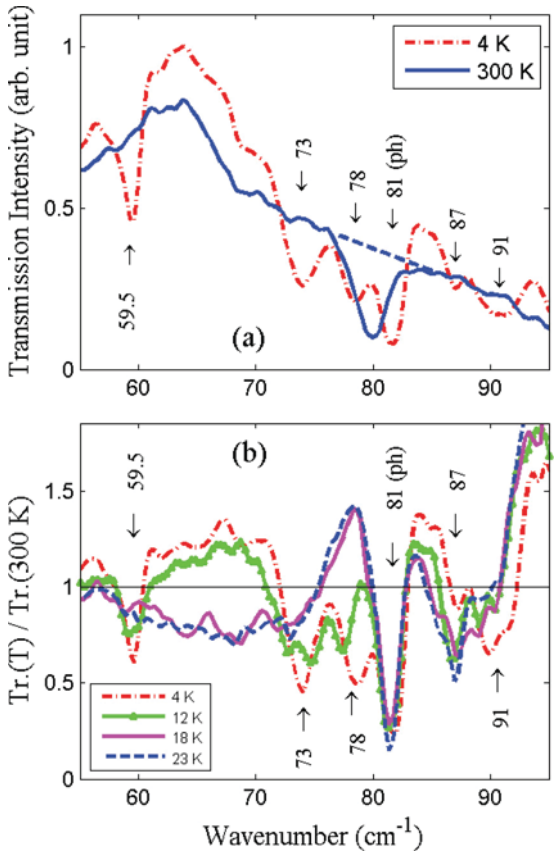

FIG. 3. (Color online) (a) Far-IR transmission spectra Tr.(T) for $Dy_3Fe_5O_{12}$ sample with $d = 0.19$ mm measured in a zero external magnetic field at $T = 4$ K (red) and $T = 300$ K (blue) . Dashed blue line shows the contribution of the optical phonon at 80 cm^{-1} to the transmission intensity at $T = 300$ K. (b) Spectra of the transmission intensity Tr.(T), which were measured at $T = 4$, 12, 18, and 23 K and normalized by that measured at $T = 300$ K: Tr.(T)/ Tr.(300 K). The arrows in (a) and (b) show the position of the LF, CF, and KK absorption lines and the phonon (ph) for $T = 4$ K. The corresponding transition frequencies in cm^{-1} are shown next to the vertical arrows.

energies of the CF transitions of Dy were reported for other garnets. For example, in Y-Ga-garnet the lowest crystal-field transitions of Dy impurities are at 20.5, 71, and 117 cm^{-1}.[32] The intensity of the CF absorption lines increases with the temperature decrease and the lines become narrower. This behavior is typical for CF transitions due to the effects of the thermal repopulation of the CF levels of Dy^{3+} and interaction between $4f$ electronic states and acoustic phonons. The CF1 line at 20 cm^{-1} [Fig. 4(a)] becomes very weak for $T > 40$ K due to thermal population of the first excited CF1 level for the temperature range with k_BT exceeding the splitting between the ground and CF1 levels (~20 cm^{-1}). In the temperature range between 16 K and 55 K, the CF4 line at ~71 cm^{-1} splits into two lines at 68 and 73 cm^{-1}, which are separated by about 5 cm^{-1} [see Figs. 2(d), 2(e), and 4(a)]. This splitting is most likely related to the rhombohedral distortion of the garnet lattice that appears in the same temperature range.[21] In Sec. VI we will discuss similar changes in the spectra of optical phonons, which are induced by the same rhombohedral distortion. The weak and broad absorption line at 42 cm^{-1} appears for $T > 20$ K and is probably due to the optical transition between the excited CF levels, such as CF1 and CF3. Similar interpretation may be used to explain a relatively weak absorption line at 14 cm^{-1} for $T > 20$ K. This energy is close to the distance between CF2 (53 cm^{-1}) and one of the CF4 components at 68 cm^{-1}. An additional support for this interpretation of the optical transitions at 14 and 42 cm^{-1} can be found in the magnetic field dependencies of the transmission spectra (see Sec. V for details). As we will see in the following,

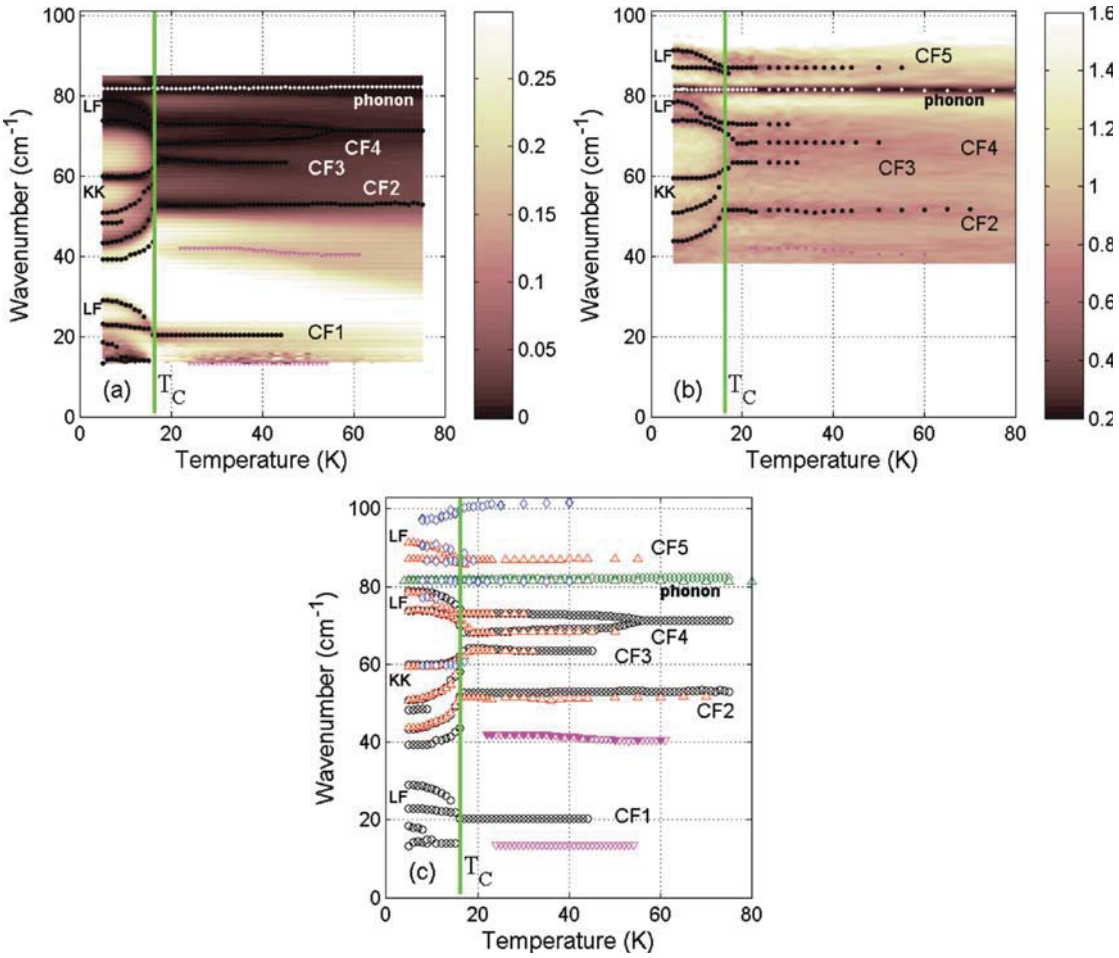

FIG. 4. (Color online) (a) Transmittivity map vs temperature and light frequency for $Dy_3Fe_5O_{12}$ sample with the thickness $d = 0.50$ mm. The transmittivity scale is between 0 and 0.3. (b) Normalized transmission intensity Tr.(T)/Tr.(300 K) vs temperature and light frequency for the same crystal as in (a) polished down to $d = 0.19$ mm. The normalized Tr.(T)/Tr.(300 K) scale is between 0.2 and 1.6. In both (a) and (b), the dark color corresponds to stronger absorption and light color indicates high transmission. The vertical green line represents the phase transition temperature $T_C = 16$ K. The white dots represent the phonon frequency at 81 cm^{-1}. Positions of the LF, CF, and KK modes are shown with black dots. (c) Frequencies of the LF, KK, and CF modes vs temperature. Data from (a) are represented by black circles; data from (b) are represented by red triangles. The green symbols represent the phonon at 81 cm^{-1}. The magenta triangles at 14 cm^{-1} and 42 cm^{-1} correspond to the optical transitions between the thermally excited CF levels: CF2 → CF4 and CF1 → CF3. The ellipsometry data for the LF transition and the phonon at 81 cm^{-1} are shown with blue diamonds.

the line at 42 cm^{-1} disappears as soon as CF1 and CF2 levels split in the external magnetic field at $T = 25$ K.

The transmission spectra for the temperature range below the phase transition for the FM order of Dy^{3+} spins at $T_C = 16$ are more complex [see Figs. 2(b), 2(c), 3(a), 3(b), 4(a), and 4(b)]. This phase transition is evident by the opening of the transparency window between 50 and 70 cm^{-1} and by a strong shift of several absorption lines away from this spectral range. For identification of the IR absorption lines we will use terms that originate from the work by Kittel *et al*. in Ref. 20. The observed far-IR absorption lines will be attributed either to the so-called Kaplan-Kittel (KK) modes or to LF exchange resonances. In the following discussion of the spectra measured for $T < T_C$ the term LF replaces CF to underline the importance of the strong exchange interaction between the ordered Dy and Fe spins which should be considered in addition to the primarily electrostatic CF interaction.

For $T = 5$ K, a number of the LF exchange resonances and KK modes appear at 13, 18, 23, 29, 39, 43, 48, 51, 59.5, 73, 78, 87, 91, and 98 cm^{-1} [Figs. 2(b), 2(c), 3(a), and 3(b)]. The transmission spectra as well as the ellipsometry spectra were fitted using a multioscillator dielectric model. The results of the fit are shown in Figs. 2(a) and 2(b) along with the experimental spectrum. Temperature dependence of the oscillator frequencies obtained from the fit is shown in Figs. 4(a)–4(c). In a zero magnetic field, the lowest-frequency absorption line at 13 cm^{-1} is very close to the edge of the measurable spectral window. However, this absorption line shifts to higher frequencies in an external magnetic field, which enables its clear identification. Figure 2(c) shows such a spectrum measured in a weak magnetic field of 10 kOe, where the peak formerly at 13 cm^{-1} shifts up by about 1.2 cm^{-1}. The complete magnetic field dependence of this absorption peak is shown in Figs. 5(a) and 5(b) and will be discussed in Sec. V. We interpret the mode at 13 cm^{-1} as due to a spin splitting

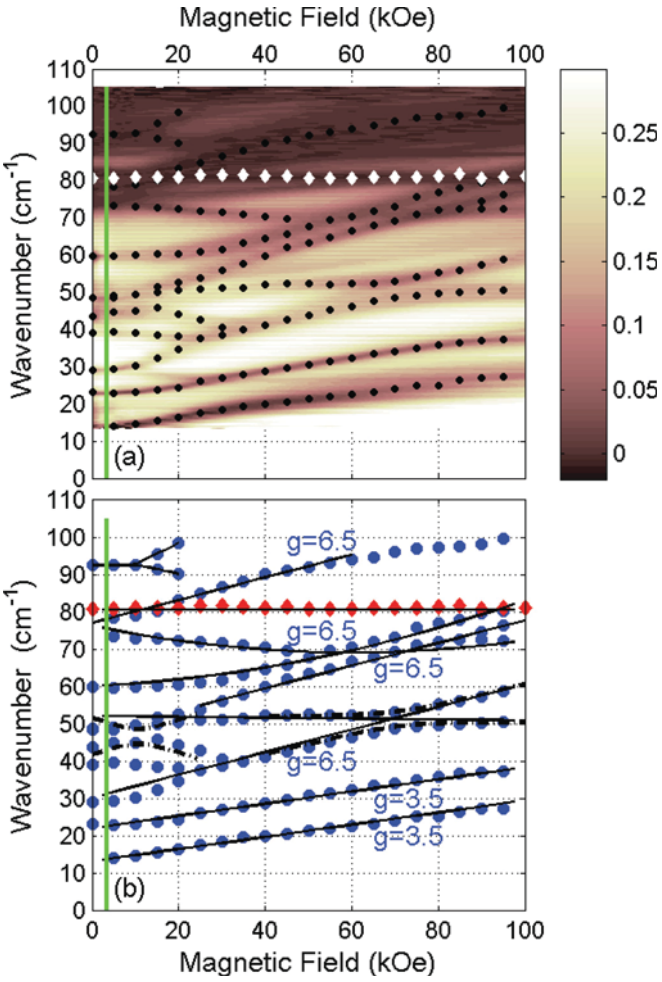

FIG. 5. (Color online) (a) Transmission map vs magnetic field and light frequency for $Dy_3Fe_5O_{12}$ at $T = 4.5$ K and $H \parallel [100]$. The dark color corresponds to stronger absorption and light color indicates high transmission. The transmission intensity scale is between 0 and 0.3. The green vertical line represents the critical field at $H_C = 3.5$ kOe. The white diamonds represent the phonon at 81 cm^{-1}. (b) Frequencies of the optical transitions vs magnetic field. The linear slopes are characterized by the g-factor values shown next to the lines. The red diamonds represent the phonon at 81 cm^{-1}.

of the ground state of Dy^{3+} ions. Several other modes at 73, 78, 87, 91, and 98 cm^{-1} are difficult for identification in the transmission spectra for a thick sample ($d = 0.50$ mm) due to significant absorption saturation in this spectral range. These peaks are much better resolved in the spectra measured for the thin sample ($d = 0.19$ mm) shown in Figs. 3(a) and 3(b). In addition, the transmission spectra have been compared with the ellipsometry data for the same sample, where the oscillators at 87, 91, and 98 cm^{-1} are seen more clearly in the spectrum for $\langle \varepsilon_1 \rangle$ [Fig. 2(a)]. The modes at 73 and 78 cm^{-1} have a hybrid or simultaneous magnetic- and electric-dipole activity, thus becoming quite weak in ellipsometry spectra (see Ref. 5 for more details). The other group of modes at 39, 43, 51, and 59.5 cm^{-1} is in the center of the measured spectral range that allows for a very accurate measurement of their frequencies. The mode at 48 cm^{-1} is very weak disappearing for $T > 10$ K that prevents its further interpretation.

The groups of KK modes at 39, 43, 51, 59.5 cm^{-1} and LF modes at 18, 23, 29, 73, 78, 87, and 91 cm^{-1} are marked in Figs. 4(a) and 4(b). The LF and KK modes can be distinguished based on their opposite temperature dependence: softening of the KK frequency and hardening of the LF frequency upon cooling down from T_C. Below we will discuss the main contributions, such as the total magnetization of the ordered Dy spins, to the temperature variation of the KK and LF frequencies and will estimate the parameters of the exchange interaction between Fe and Dy spins.

In a simplified model for a two-spin ferrimagnetic system, such as R-Fe, an exchange-type KK mode is expected with the frequency Ω_M. Another mode Ω_{LF} corresponds to precession of the Dy moments in the effective field imposed by the iron magnetization due to the superexchange interaction between Fe and R^{3+} ions. According to Refs. 20 and 29, the zone-center frequencies of these modes can be estimated in the simplified model for two interacting spins:

$$\Omega_M(T) = \lambda_{\mathrm{Fe-Dy}}\mu_B[g_{\mathrm{Dy}}M_{\mathrm{Fe}} - g_{\mathrm{Fe}}M_{\mathrm{Dy}}(T)],$$
$$\Omega_{\mathrm{LF}} = \lambda_{\mathrm{Fe-Dy}}\mu_B g_{\mathrm{Dy}}M_{\mathrm{Fe}}, \quad (1)$$

where μ_B is the Bohr magneton ($\mu_B \approx 0.04669$ cm^{-1}/kOe), $\lambda_{\mathrm{Fe-Dy}}$ is the exchange constant between Fe and Dy ions, $g_{\mathrm{Fe}} = 2$ and g_{Dy} are the corresponding g factors, $M_{\mathrm{Dy}}(T)$ is the Dy-sublattice magnetization, and M_{Fe} is the combined Fe magnetization for a and c sites. When temperature decreases below $T_C = 16$ K, the KK modes exhibit softening of the frequency $\Omega_M(T)$ due to increase of the Dy magnetization $M_{\mathrm{Dy}}(T)$. Note that $M_{\mathrm{Dy}}(T)$ is zero for $T > T_C$ and frequencies of the KK and LF modes should coincide in this case with that for an unperturbed CF transition energy. Figures 2(b), 4(a), and 4(c) show three KK modes at 39, 43, and 51 cm^{-1}, that can be explained by the presence of two types of Dy spins in the double umbrella structure and by the strongly anisotropic and temperature-dependent superexchange interaction between Dy and Fe ions. The mode at 59.5 cm^{-1} seems to be nearly temperature independent up to ~14 K. However, between 14 and 16 K this mode also increases the frequency by a few cm^{-1}, thus showing a typical KK-type behavior at the phase transition.

The temperature-induced variation of the frequency for the KK modes mode below 16 K is equal to $\Delta\Omega_M(T) = -\lambda_{\mathrm{Fe-Dy}}g_{\mathrm{Fe}}\mu_B M_{\mathrm{Dy}}(T)$, which is proportional to magnetization of Dy spins. The shape of the curves for $\Omega_M(T)$ in Fig. 4(c) corresponds to a phase transition with the appearance of the long-range ordering of Dy spins below $T_C = 16$ K, rather than a gradual change as expected for a paramagnetic (PM) moment in the effective field. The relatively sudden appearance of the Dy magnetic phase below 16 K indicates that the Dy-Dy exchange interaction energy is not small compared to that for Fe-Dy exchange, possibly due to the large and anisotropic g factor of Dy ions g_{Dy}. The literature values of the g_{Dy} tensor components are $\{11.07, 1.07, 7.85\}$, two of which are significantly larger than that for the $^6H_{15/2}$ free-ion ($g_{^6H_{15/2}} = 4/3$).[21] Note that such a difference is common in R-IGs, where the J mixing and repopulation of the CF states at low temperature modify the effective g factor, making it strongly anisotropic.

Three groups of LF modes, centered above 20, 70, and 90 cm^{-1}, have a trend that is opposite to that for the KK modes with their frequencies decreasing with the temperature

increase between 5 and 16 K. This trend is not typical for single-ion transitions in the effective field produced by Fe ions, which predicts a temperature-independent behavior for Ω_{LF} in Eq. (1). Note that the observed $\Omega_{LF}(T)$ is similar to the temperature dependence of the exchange mode previously measured in another R-IG: $Er_3Fe_5O_{12}$.[28] As inferred from the shape of $\Omega_{LF}(T)$ in Fig. 4(c) for several LF modes above 20, 70, and 90 cm^{-1}, their temperature dependence should be also influenced by the Dy-Dy exchange interaction. By representing the exchange interaction between Dy^{3+} ions with the FM exchange constant λ_{Dy-Dy}, Sievers and Tinkham derived the expression for the temperature-dependent LF energies[28]

$$\Omega_{LF}(T) = g_{Dy}\mu_B[\lambda_{Fe-Dy}M_{Fe} + \lambda_{Dy-Dy}M_{Dy}(T)], \qquad (2)$$

which should replace the bottom line in Eq. (1) for materials with a strong FM exchange constant λ_{Dy-Dy}. The temperature-dependent part of the LF mode frequency is $\Delta\Omega_{LF}(T) = \lambda_{Dy-Dy}g_{Dy}\mu_B M_{Dy}(T)$, which has the opposite sign compared to $\Delta\Omega_M(T) = -\lambda_{Fe-Dy}g_{Fe}\mu_B M_{Dy}(T)$ for the KK modes. Although it is known that the exchange constant between Fe and R ions is significantly larger than that for the Dy-Dy interaction,[21] a relatively large value of g_{Dy} compared to $g_{Fe} = 2$ can make $|\Delta\Omega_{LF}(T)|$ comparable to $|\Delta\Omega_M(T)|$ in Dy-IG. The strong anisotropy of the g-factor tensor for Dy explains why more than one absorption line $\Omega_{LF}(T)$ is observed for each CF energy level above 20, 70, and 90 cm^{-1}. From the comparison between the changes of the LF excitation frequencies $\Delta\Omega_{LF}(5\text{ K}) = 7$ cm^{-1} and $\Delta\Omega_M(5\text{ K}) = -10$ cm^{-1} with respect to their values for $T \approx T_C$, we can estimate the ratio of the coupling constant for Dy-Fe and Dy-Dy interactions. Taking the literature values of $g_{Dy} \approx 11$ and $g_{Fe} = 2$, we obtain $\lambda_{Dy-Dy}/\lambda_{Fe-Dy} = 0.13$. In this estimate we did not take into account possible Fe spin reorientation.[25] A more elaborate theoretical model may be needed to include temperature dependence of M_{Fe} below 16 K.

Note that according to the simplified model for collinear Dy^{3+} and Fe^{3+} spins that was developed in Refs. 20 and 29 for R-IGs, the KK and LF exchange-resonance modes are collective excitations of Dy^{3+} and Fe^{3+} spins with spatial dispersion. On one hand, they can be viewed as pure magnons which contribute only to the magnetic permeability $\mu(\omega)$.[29] In Ref. 5 we studied the type of the dipole activity of the LF and KK modes experimentally using a combination of several optical techniques: transmission and reflectivity at normal incidence, and RAE. It turns out that the KK modes are primarily magnetic dipoles, while the LF modes have a hybrid or a simultaneous electric- and magnetic-dipole activity. Thus the LF modes can contribute to both static values of $\varepsilon(0)$ and $\mu(0)$. The electric dipole activity of the LF modes originates primarily from their proximity to the frequencies of the optical phonons the lowest of which is at 81 cm^{-1}. In the following section we will discuss spectra of the KK and LF modes in external magnetic field.

V. EXPERIMENTS IN MAGNETIC FIELD

A. Strong magnetic field

Figure 5(a) shows maps of the transmission intensity vs magnetic field for $T = 4.5$ K. The frequencies of the phonon, KK, and LF modes are shown in Fig. 5(b). As expected, the lowest optical phonon at 81 cm^{-1} does not change its frequency in the external magnetic field. In contrast, a strong magnetic field H applied along the [100] direction in the Faraday configuration causes an increase of the KK and LF frequencies. In the high-field regime, this effect can be described by the effective g factors as follows: $\Omega(H) = \Omega(0) + g\mu_B H$, where μ_B is the Bohr magneton ($\mu_B \approx 0.04669$ cm^{-1}/kOe). The corresponding slope $\partial\Omega(H)/\partial H = g\mu_B$ for the lower-frequency transitions at 13 cm^{-1} is close to $3.5\mu_B$, while for the higher frequency modes the slope is about $6.5\mu_B$ [see Fig. 5(b)]. One can compare these values to the effective g_{Dy} tensor components for Dy^{3+} in Dy-IG: $\{g_x = 11.07, g_y = 1.07, g_z = 7.85\}$, which were measured in the x-y-z coordinate system aligned with respect to the magnetization direction for Fe spins.[21] For our experiment, where H is applied along the [100] crystallographic direction, the corresponding g factors have to be recalculated based on these literature values of g_{Dy}. By applying this coordinate rotation for the g-factor tensor, we obtained the modified slope values of $3.6\mu_B$ and $5.7\mu_B$ for magnetic field along [100]. These numbers are reasonably close to our experimental results in Fig. 5(b): $3.5\mu_B$ and $6.5\mu_B$.

In the temperature range above the Dy FM phase transition $T > 16$ K, the number of the IR-active modes decreases compared to that at low temperatures. The corresponding magnetic field dependence of transmission is shown in Figs. 6(a) and 6(b) for $T = 25$ K. There are two groups of absorption lines in the diagram. At zero magnetic field, one group of lines originates from the CF1 level at 20 cm^{-1}, and another one originates from the CF2 level at 53 cm^{-1}. Each group of lines consists of three modes that have the slope values of about zero, $5.5\mu_B$, and $9.5\mu_B$, respectively. Thus, the temperature maps shown in Fig. 4(a) and the magnetic field maps in Figs. 5(a) and 6(a) can be qualitatively reconciled as follows. At zero magnetic field and high temperature, the low-frequency part of the spectrum is dominated by the CF lines at 20 and 53 cm^{-1}. Each line is a multiplet with the effective g-factor values of about zero, 5.5, and 9.5. Upon zero-field-cooling through the phase transition at $T_C = 16$ K, the CF1 and CF2 modes at 20 cm^{-1} and 53 cm^{-1} split into several LF lines. For example, the low-frequency one at 20 cm^{-1} splits into two modes at 22 and 29 cm^{-1} [see Figs. 4(a) and 4(c)] with g factors of 3.5 and 6.5, respectively [see Figs. 5(a) and 5(b)]. The effective magnetic field values that cause the corresponding frequency shift by 2 and 9 cm^{-1} are $H_{ef1} = 12$ and $H_{ef2} = 30$ kOe. In turn, these values of the effective magnetic field correspond to the LF contribution to the CF caused by the Dy-Dy ordering below 16 K. Note that due to the strong temperature dependence of g_{Dy}, this estimate is applicable to the low temperatures only.

B. Weak magnetic field

Figure 7(a) shows the magnetic field dependence of the quasistatic value of the dielectric constant. As we reported recently in Ref. 5, $\varepsilon(0, H)$ has a peak at $H = 1$ kOe at $T = 5$ K. For higher magnetic fields, $\varepsilon(0, H)$ slowly decreases with H. This dependence is invariant with respect to the sign of external magnetic field. The magnetization curve which is shown in Fig. 7(b) has a pronounced step in the same range of magnetic

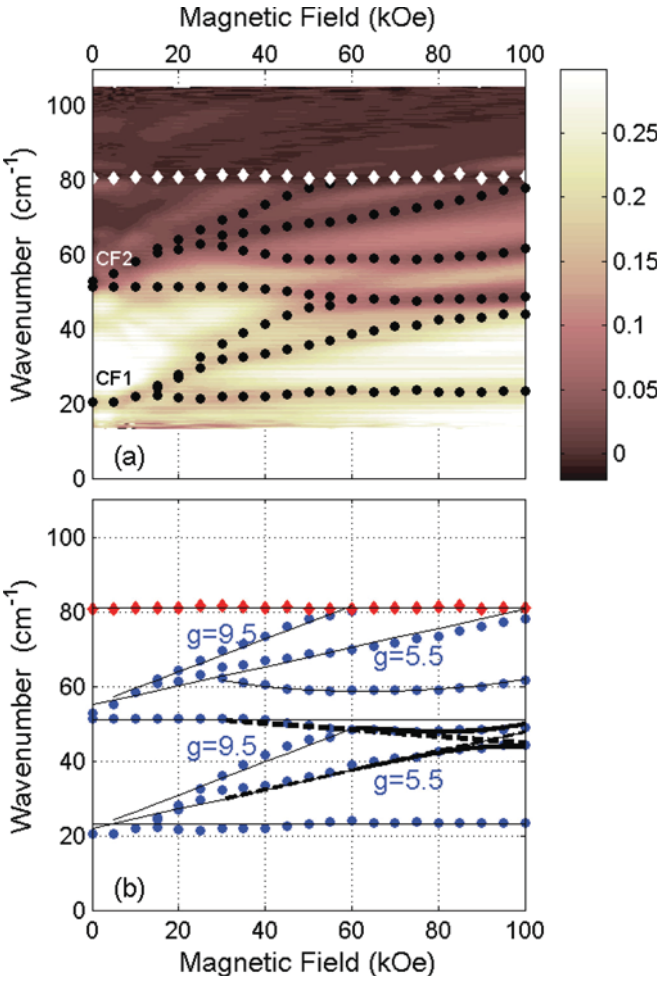

FIG. 6. (Color online) (a) Maps of the normalized transmitted intensity vs magnetic field and frequency for $Dy_3Fe_5O_{12}$ at $T = 25$ K and $H \parallel [100]$. The dark color corresponds to stronger absorption and light color indicates high transmission. The transmission intensity scale is between 0 and 0.3. The white diamonds represent the phonon at 81 cm^{-1}. (b) Frequencies of the optical transitions vs temperature. The linear slopes are characterized by the g-factor values shown next to the lines.

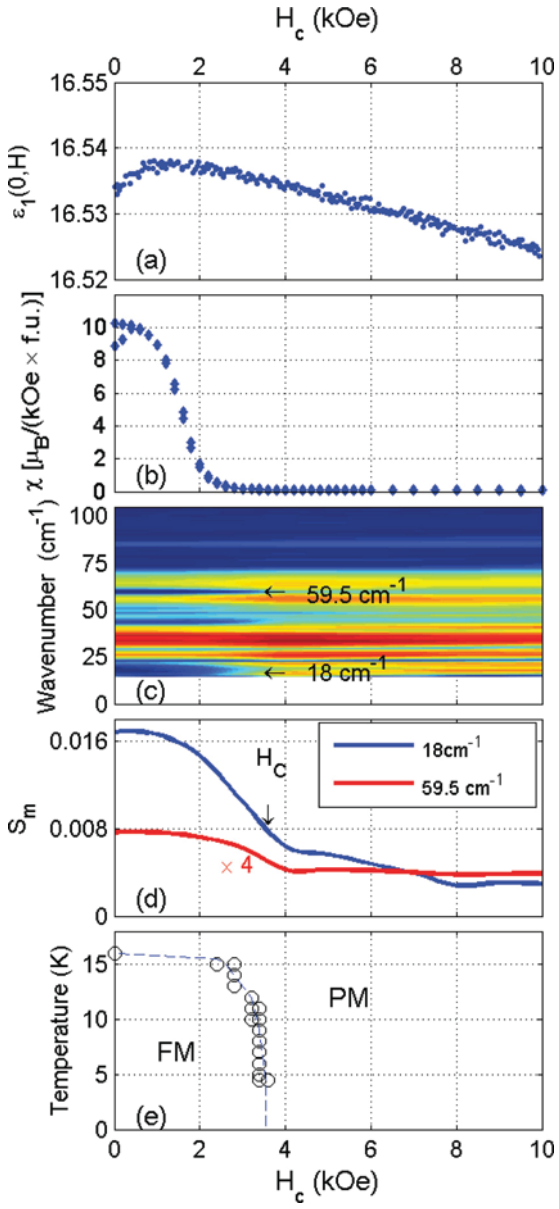

FIG. 7. (Color online) (a) Magnetic field dependence of the static dielectric constant at $T = 5$ K, $E \parallel [100]$ and $H \parallel [011]$ from Ref. 5. (b) Magnetization curve with a small splitting at low field due to initial magnetization. (c) Transmission map vs magnetic field and light frequency for $Dy_3Fe_5O_{12}$ at $T = 4.5$ K and $H \parallel [100]$. The blue (dark) color corresponds to stronger absorption while red (light) color indicates high transmission. The transmission intensity scale is between 0 and 0.3. (d) Oscillator strength vs magnetic field. The critical field is marked with arrow. (e) The FM-PM phase diagram based on the values of the oscillator strength vs T-H.

field. In the following we will discuss the connection between $\varepsilon(0, H)$ and the far-IR excitations, i.e., LF and KK modes.

Figure 7(c) shows a transmission intensity map for weak magnetic fields at $T = 4.5$ K. The effective oscillator strength $S_T(H)$ for the LF mode at 18 and KK modes at 43, 51, and 59.5 cm^{-1} decreases strongly when the field exceeds ~3.5 kOe, while the modes at 22, 29, 73, and 78 cm^{-1} remain practically unchanged. Modification of the oscillator strength for the modes at 18 and 59.5 cm^{-1} is shown in Fig. 7(d), where the value of the critical field $H_C = 3.5$ kOe corresponds to the inflection point for $S_T(H)$. In the vicinity of the phase transition at $T_C = 16$ K, the critical field depends on the sample temperature. The phase diagram that is based on the oscillator strength dependence on the field and temperature, $S_T(T, H)$, is shown in Fig. 7(e) for the modes at 18 and 59.5 cm^{-1}. We assign the lower left corner to the FM phase for Dy-Dy spins, while the PM phase is in the upper right section for high temperatures and high magnetic fields.

In principle, the magnetic-field-induced variation of the oscillator strength $S_T(T, H)$ for the KK and LF modes can contribute to the static values of $\varepsilon(0)$ or $\mu(0)$ depending on the dipole activity of each mode. In Ref. 5 we demonstrated how a combination of the reflection and transmission techniques can be used to identify the dipole activity of the IR-active modes. The effective oscillator strength of the modes of the hybrid activity determined from transmission experiments is $S_T \approx \mu_\infty S_e + \varepsilon_\infty S_m$, where ε_∞ and μ_∞ are the high-frequency

values and $S_{e,m}$ are the true values of the oscillator strength for the electric and magnetic components of the hybrid modes. Naturally, $\mu_\infty \cong 1$, while $\varepsilon_\infty \cong 17$ for Dy-IG in the frequency range below all optical phonons (<80 cm^{-1}).[5] From our previous studies of Dy-IG,[5] the KK mode at 59.5 cm^{-1} in Fig. 2(b) is a pure magnetic dipole contributing only to $\chi(0,T)$ shown in Fig. 1(a). The type of dipole activity for other lower frequency modes (below 55 cm^{-1}) was not determined in Ref. 5 due to their insufficient intensity in the reflectivity experiments. Since we cannot unambiguously separate the oscillator strength contribution of the modes at 18, 43, and 51 cm^{-1} between $\varepsilon(0)$ and $\mu(0)$, the indirect reasons can be utilized for identification of their dipole activity. On one hand, the $\varepsilon(0,H)$ dependence shown in Fig. 7(a) does not directly correlate with the oscillator strength of the LF modes at 18, 43, and 51 cm^{-1}. On the other hand, the magnetic field dependence of the sample magnetization, which is presented in Fig. 7(b) in terms of $\chi(H) = \partial M(H)/\partial H$, correlates well with the magnetic-field-induced decrease of the oscillator strength for the modes at 18, 43, 51, and 59.5 cm^{-1}. Thus, we can conclude that the LF mode at 18 and KK modes at 43 and 51 cm^{-1} are predominantly magnetic, the same as the KK mode at 59.5 cm^{-1}. The oscillator strength change for those magnetic modes is shown in Fig. 7(d) in units of S_m that are related to the static value of $\mu(0,H)$ as follows: $\mu(0,H) = 1 + \chi(0,H) = 1 + \sum_i^N S_{m,i}(H)$, where summation is taken for N magnetic modes. We conclude that the oscillator strength changes S_m are associated with the FM-PM phase transition at 3.5 kOe rather than with the AFE behavior for $\varepsilon(0,T)$ in Fig. 1(b).

In Ref. 5 we demonstrated that the modes at 73, 78, and 91 cm^{-1} are of a hybrid origin, possessing both electric and magnetic dipole activities. However, these modes, which could contribute directly to the change of $\varepsilon(0,H)$ in Fig. 7(a), did not show any appreciable change of their frequency or their oscillator strength at 1 kOe [see Fig. 7(c)]. Thus, we conclude that the magnetodielectric effect in Dy-IG is not directly related to any of the measured low-frequency LF or KK modes, but is rather determined by the optical phonons.

VI. SPECTRA OF THE OPTICAL PHONONS

Spectra of the optical phonons in R-IG were previously studied both theoretically and experimentally.[33–35] The group theory analysis predicts 17 IR-active optical modes in R-IGs at room temperature.[34] Most of the optical phonons have been already observed using transmission spectroscopy in polycrystalline samples.[34] However, due to limitations of the traditional transmission technique, no details are available in the literature on the temperature dependence of the phonon frequency, broadening, and oscillator strength for Dy-IG. In this section we present our experimental results for the optical phonon spectra obtained with high spectral resolution and small temperature steps around T_C. Modification of the phonon spectra due to rhombohedral distortions for $T < 100$ K will be discussed. We will show that the temperature dependence of $\varepsilon(0,T)$ in Fig. 1(b) correlates with the oscillator strength of the low-frequency IR-active optical phonons, which also has a peak in the oscillator strength at $T_C = 16$ K.

Figure 8 shows experimental data for the real and imaginary parts of the dielectric function ε_1 and ε_2 for 8 K and 300 K

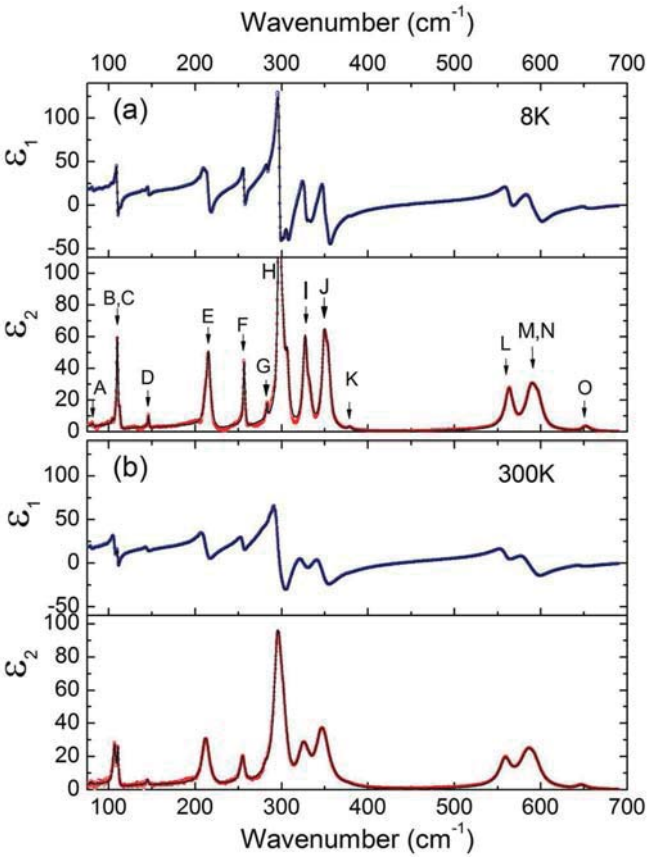

FIG. 8. (Color online) Real ε_1 and imaginary ε_2 parts of the dielectric function for Dy-IG with [100] orientation measured with AOI = 75°. Experimental results are shown with dots. The results of the fit are shown with solid black curves. (a) $T = 8$ K, (b) $T = 300$ K. The phonon modes are marked with arrows and denoted with letter symbols from A to O in the order of their frequency increase. The maximum value of ε_2 for the H phonon at $T = 8$ K, which is off the vertical scale, is 195.

obtained using RAE. The spectra of the dielectric function were fitted with a model function consisting of a set of Lorentz oscillators:

$$\varepsilon(\omega) = \varepsilon_\infty + \sum_{j=1}^{N} \frac{S_j \omega_{j,0}^2}{\omega^2 - \omega_{j,0}^2 - i\gamma_j \omega}, \qquad (3)$$

where $\omega_{j,0}$ is the phonon frequency, S_j is the oscillator strength, γ_j stands for the phonon broadening, and ε_∞ represents the dielectric constant at frequencies above the optical phonons. Two fitting programs have been consistently used for data analysis: commercial WVASE32 Woollam software and a homemade program based on the 4 × 4 Berreman's model for anisotropic magnetoelectric medium.[36] For the spectra measured at low temperatures, the maximum number of the oscillators used in the fit was $N = 27$. This number does not include the numerous CF and LF transitions below 80 cm^{-1} that were already described in the previous section. Eight weak modes, which correspond to the CF excitations of Dy^{3+}, vanish for the temperatures above ~50 K. To describe the optical phonon spectrum we used $N = 19$ oscillators for $T <$ 125 K and $N = 15$ oscillators for $T > 125$ K. The results of the

TABLE I. Parameters of the fit of the experimental RAE spectra for the optical excitations in Dy-IG between 80 cm^{-1} and 700 cm^{-1} for two temperatures: 8 and 300 K. Results from Ref. 34 are shown for comparison. The optical phonon peaks are numbered (left column) and labeled with letters A to O according to the increase of the mode frequency. The type of the modes, such as phonon (Ph) or crystal field (CF), is shown in the right-hand column. Phonons that split at low temperature into two modes are marked with Ph(2). The weak modes are marked with stars next to their frequencies.

		ω_0 (cm^{-1}) $T = 8$ K	ω_0 (cm^{-1}) $T = 300$ K	ω_0 (cm^{-1}) $T = 300$ K[a]	S $T = 300$ K	γ (cm^{-1}) $T = 300$ K	Type
1	A	81	79.7		0.07	1.8	Ph
		98*					CF
		104*					CF
		107.5*					CF
2	B	110	106.5	108	0.90	3.8	Ph
3	C	113	110.5	111	0.38	1.8	Ph
		114*					CF
		119*					CF
		123*					CF
4	D	146	144.8		0.12	3.8	Ph.
		139.8*					CF
		205*					CF
5	E	211*					
		215	211	215	1.43	7	Ph (2)
6	F	256.7	255	255	0.43	6	Ph
7	G	283*	281		0.05	5	Ph
8	H	298	296	309	3.8	9	Ph (2)
		307*					
9	I	327	324	330	0.80	10	Ph (2)
		332*					
10	J	349	347	365	1.7	15	Ph (2)
		354*					
11	K	379*	377.5*	380	0.03	5	Ph
		442*					LO
12	L	563	559	562	0.48	17	Ph
13	M	589	585		0.75	23	Ph
14	N	597	594	597	0.20	15	Ph
15	O	653	645	647	0.03	10	Ph

[a]Data from Ref. 34.

fit are shown in Figs. 8(a) and 8(b) with solid curves. A good agreement between the fit and experimental data was obtained after applying a standard data correction for the light focusing on the sample with the numerical aperture $F/10$ used in our experiment.

The optical spectra of $\varepsilon_{1,2}(\omega)$ are dominated by several strong IR phonons that are marked in Fig. 8(a) with the capital letters in the order of their frequency increase. The experimental values of the phonon parameters are summarized in Table I. The phonons labeled A, D, F, G, L, and O are single peaks and their frequencies are close to what have been previously determined from transmission experiments in polycrystalline samples.[34] Other modes, such as E, H, I, and J, are closely spaced doublets at $T < 125$ K, which converge into single peaks at higher temperatures. Two phonon modes B and C are well resolved up to room temperature. The high-frequency phonons M and N are close to each other and their separation at room temperature becomes less than their broadening. We still consider the M and N modes as separate phonons since their splitting is well defined in the spectra of the frequency derivative of $\partial[\varepsilon_1(\omega)]/\partial\omega$. Note that in the earlier transmission measurements the weak G mode was not detected and the splitting between M and N peaks was not included in consideration, and these two phonons were identified as single modes.[34] That explains why only 13 IR phonons were previously reported for R-IGs, while 17 phonons are predicted by the group theory analysis. In this paper we identify 15 phonon modes: from A to O. The possible candidates for the two missing optical phonons at room temperature are probably among the unresolved E, H, I, and J doublets. Note, however, that each of these four modes could be well described with single oscillators with some shape distortions due to anharmonic interaction with other optical and acoustic phonons. Future measurements of other R-IG compounds should help us to identify the frequencies of the two missing optical phonons.

Figures 9–11 show temperature variation of the phonon frequency, broadening, and oscillator strength. Parameters of the strong modes are shown with solid symbols, while the temperature dependence of the weaker modes is presented with open symbols. The high-frequency phonons, which are associated with vibrations of the lighter ions (oxygen and iron), have a weak frequency dependence at $T < 95$ K and a typical decrease of their frequency with the linear slope for

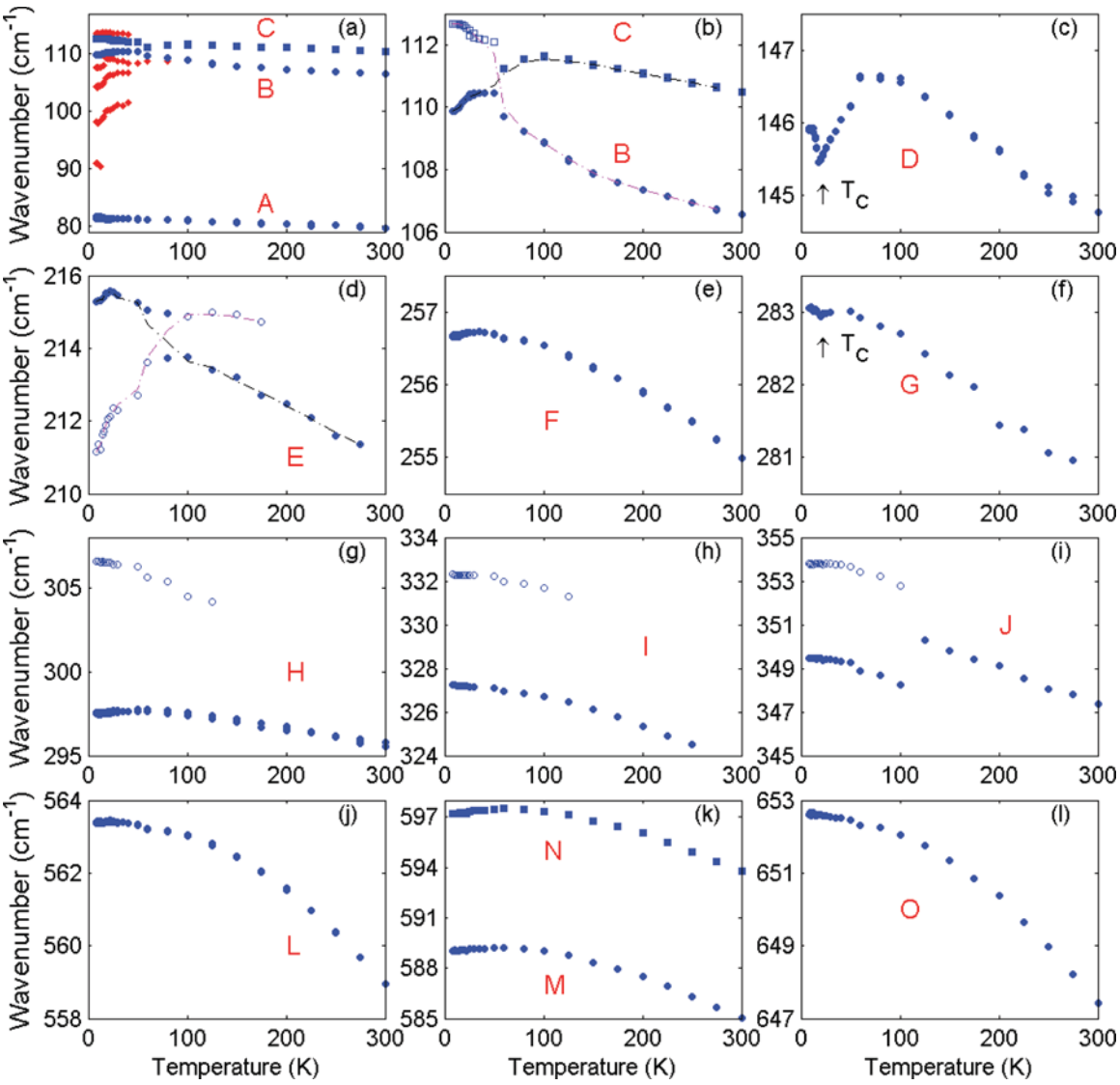

FIG. 9. (Color online) Temperature dependence of the frequency for the optical phonons, LF and CF modes. Weak phonon modes are shown with open symbols; strong modes are shown with solid symbols. Letters correspond to the phonon notation in Table I. (a) A, B, and C phonons. Positions of several weak LF and CF peaks at $T < 45$ K are shown with red diamonds. (b) A closer view at the B and C phonons. The dashed curves guide the eye for the anticrossing between B and C modes at $T = 70$ K. (c) D phonon, (d) E phonon that splits into two modes below $T = 125$ K. The dashed curves guide the eye for the anticrossing between two components at $T = 70$ K. (e) F single phonon. (f) G single phonon. (g) H phonon that splits into two modes at $T < 125$ K. (h) I phonon that splits into two modes at $T < 125$ K. (i) J phonon that splits into two modes at $T < 125$ K. (j) L single phonon. (k) M and N phonons. (l) O single phonon.

$T > 150$ K. This natural softening of the optical modes with the temperature increase is caused by the thermal expansion of the lattice and anharmonic phonon-phonon interactions, which become more important as the temperature increases due to the statistical increase of the number of acoustic phonons. In the high-temperature regime, the oscillator strength of the phonons does not change strongly with temperature, while the damping increases quasilinearly with temperature (see Fig. 10).

The errors for the phonon parameters in Table I depend on the type of the mode. For example, the frequencies of the strong single modes, such as D and F, have been determined with uncertainty of about ± 0.1 cm^{-1}. The uncertainty increases, of course, for the frequencies of the broad and weak modes, such as G, L, and O, to about ± 0.3 cm^{-1}. The components of the doublets, such as E, H, I, and J, may have a larger uncertainty for the frequency of the individual components due to instability of the fitting procedure for the overlapping peaks. The errors for the phonon broadenings is about ± 0.2 cm^{-1} for strong single modes and ± 0.5 cm^{-1} for the weak ones. The oscillator strength is the least stable parameter in RAE measurement. For weak modes, the absolute value of the oscillator strength may have an uncertainty exceeding 20% that is determined by the nature of the nonlinear conversion between the measured ellipsometric angles Ψ, Δ and the dielectric function components: $\{\Psi, \Delta\} \rightarrow \{\varepsilon_1, \varepsilon_2\}$. Even the strong modes may sometimes have a large uncertainty in their oscillator strength due to, for example, the proximity of the experimental values of Δ to 0 or 180°. Note, however,

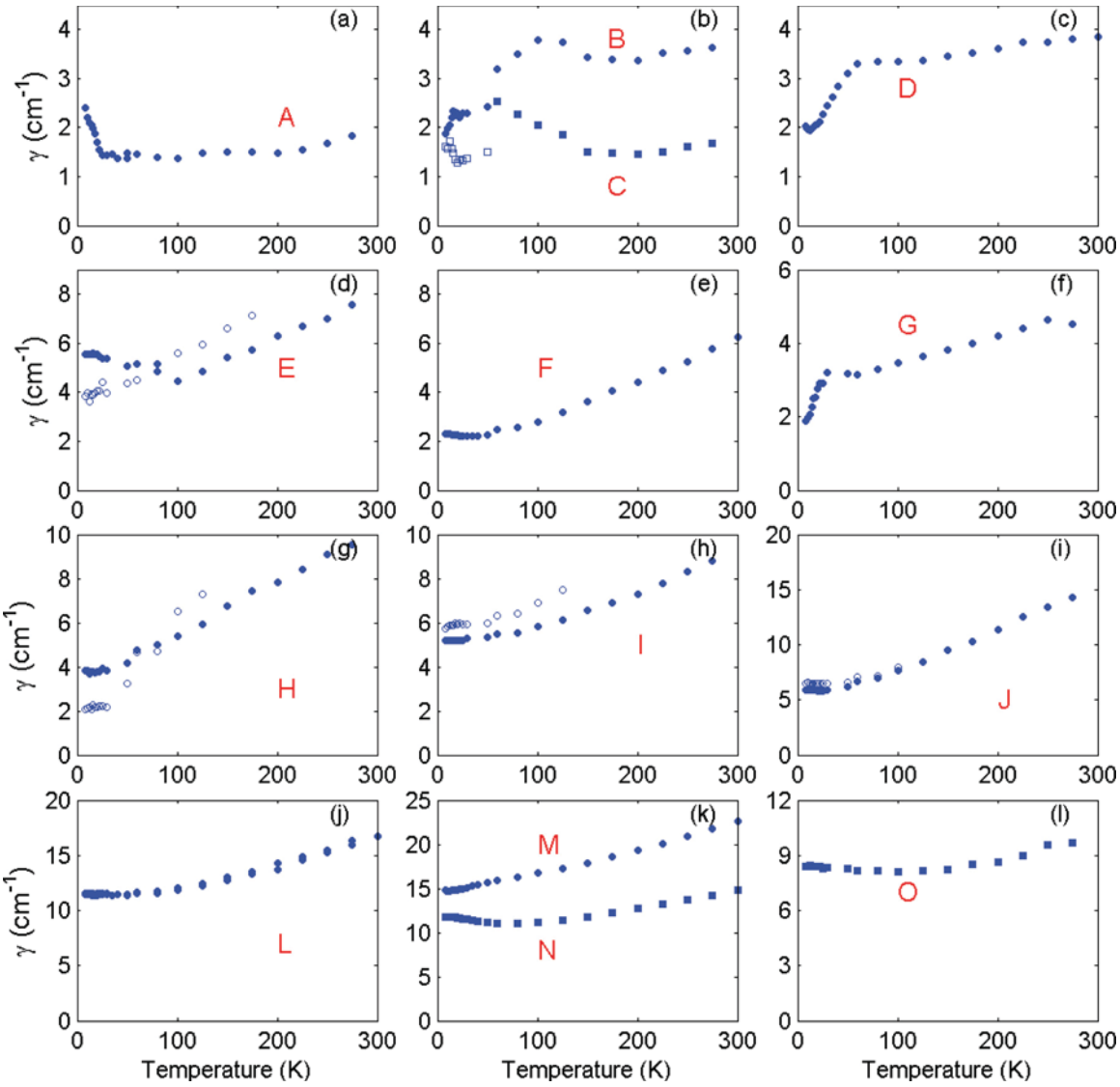

FIG. 10. (Color online) Temperature dependence of the optical mode broadening γ. Data for the weak phonon modes are shown with open symbols; strong modes are represented by solid symbols. Letters correspond to the mode notation in Table I. The subplot position is the same as in Fig. 9.

that the relative changes of the oscillator strengths with temperature, as well as the relative temperature-induced shifts of the mode frequencies, which are the focus of this paper, have been measured more accurately than their absolute values.

As we have already seen in Sec. IV of this paper, the lowest frequency optical phonon in Dy-IG is at 81 cm^{-1} [peak A in Fig. 8(a)]. This phonon is related to the $R-$ion motion and is significantly weaker than the IR optical phonons with the frequencies higher than 100 cm^{-1}. The other two low-frequency phonons, B and C, which are also associated with vibrations of the heaviest ion (Dy^{3+}), revealed a fine structure around the primary peaks [Fig. 9(a)]. At low temperatures the B and C phonons at ~110 and 113 cm^{-1} are surrounded by several weak modes at 98, 104, 107.5, 114, and 119 cm^{-1}. Our modeling approach, which can handle the contribution of both electric and magnetic dipoles (see Ref. 5 for details), shows that all peaks at 98, 104, 107.5, 114, and 119 cm^{-1} can be attributed to electric-dipole active LF and CF excitations. These excitations have anomalous temperature dependence of their frequency for $T < 45$ K. Above 50 K, when most of the CF peaks vanish due to both the temperature-induced depletion of the ground state and to disappearance of the AFE ordering, the phonons B and C form a doublet with two components of comparable strength that are separated by ~5 cm^{-1}. Note that the frequency and oscillator strength dependencies in Figs. 9(b) and 10(b) suggest an anticrossing between these two modes at $T = 70$ K.

The E phonon at ~215 cm^{-1} splits into two lines at low temperatures $T < 125$ K, which in turn experience an anticrossing at $T = 70$ K as shown in Figs. 9(d) and 12(a). The splitting for the E phonons, as well as that for the H, I, and J phonons in Figs. 9(g)–9(i), correlates with the rhombohedral distortion of the cubic cell [see Fig. 12(b)] reported previously for Dy-IG in the same temperature range.[21] Calculations of the temperature dependence of the E phonon frequency has been

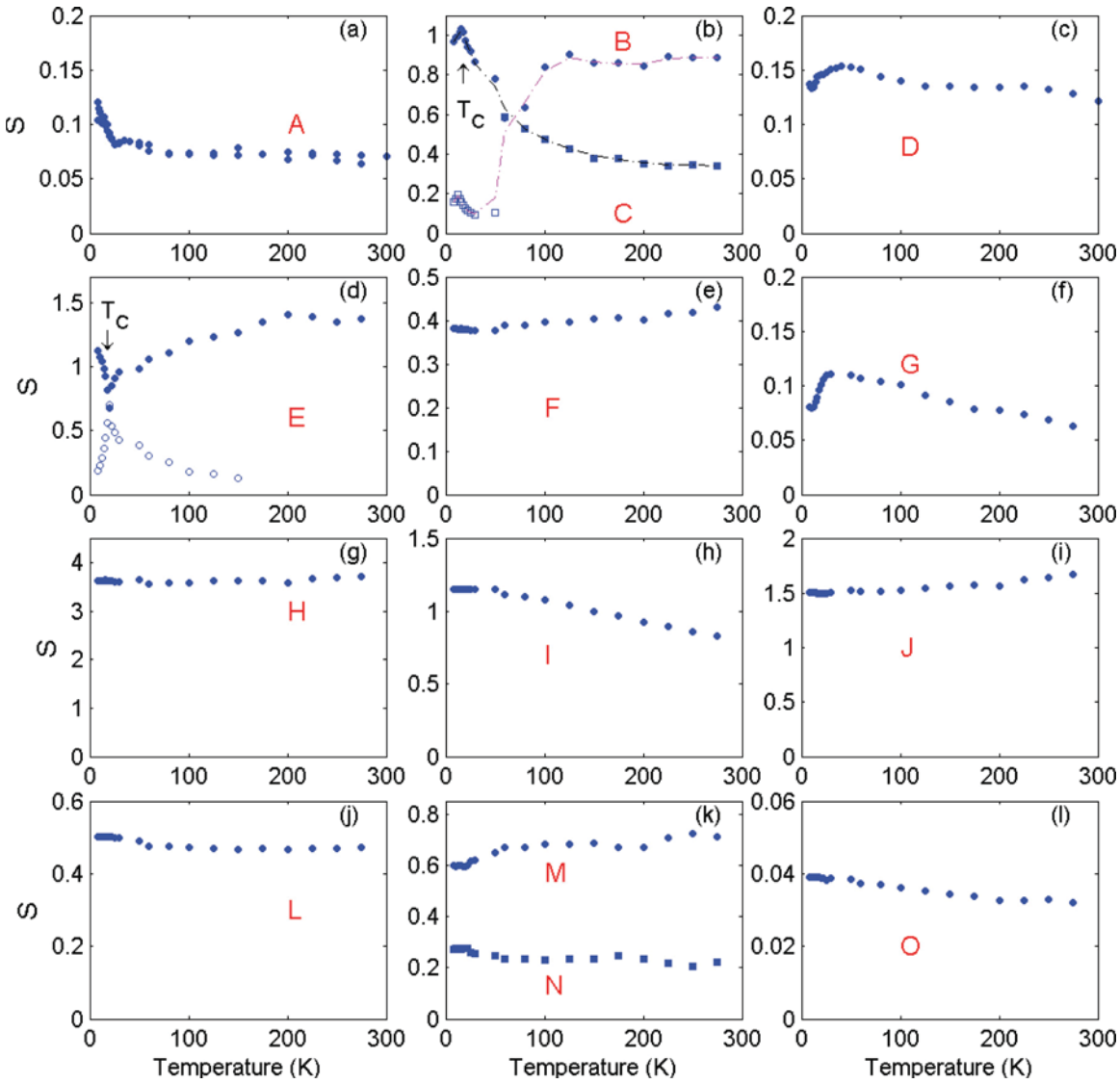

FIG. 11. (Color online) Temperature dependence of the oscillator strength S. The weak phonon modes are shown with open symbols; strong modes are shown with solid symbols. Letters correspond to the mode notation in Table I. The subplot position is the same as in Fig. 9. The dashed curves in (b) guide the eye for the oscillator strength transfer between B and C modes. Subplots (g), (h), and (i) show the average values of S for the H, I, and J doublets.

done using the equation[37]

$$\omega_0(T) = \omega_{0|T=0} \exp\left[-3\gamma_G \int_0^T \alpha(T')dT'\right], \qquad (4)$$

where γ_G is a Grüneisen parameter, $\alpha(T)$ is the linear expansion coefficient obtained from Ref. 21 [the corresponding experimental data are shown in Fig. 12(b)], and $\omega_{0|T=0}$ is the phonon frequency at zero temperature. The results of the calculation using $\gamma_G = 0.7 \pm 0.2$ and $\omega_{0|T=0} = 214$ cm^{-1} are shown in Fig. 12(a) with a solid curve. While the high-temperature regime for $\omega_0(T)$ is well described by Eq. (4), the same formula cannot be directly applied in the low-temperature range ($T < 70$ K) for the lattice that is significantly affected by the rhombohedral distortion. Nevertheless, we note that both the thermal expansion of the lattice and anharmonic phonon-phonon interaction can result only in an increase of the phonon frequency with the temperature decrease. Thus, these two conventional mechanisms cannot explain the softening of the low-frequency component of the E mode below $T \approx 70$ K, which may be an indication that the AFE phase is formed in the sample at low temperatures.

An additional indication of the AFE phase formation can be found in the temperature dependence of the frequency for the D phonon $\omega_{D,0}(T)$[Fig. 9(c)]. $\omega_{D,0}(T)$ has a sharp minimum at $T_C = 16$ K, where $\omega_{D,0}(T)$ decreases from ~146.7 cm^{-1} at $T = 50$ K to 145.5 cm^{-1} at $T = 16$ K and recovers back to 146 cm^{-1} at $T = 8$ K. This trend for $\omega_{D,0}(T)$ contradicts what is expected from conventional thermal expansion [Eq. (4)] and may also indicate an appearance of electric polarization at low temperatures with the maximum at $T_C = 16$ K. Since our dc measurements did not reveal any measureable macroscopic electric polarization in Dy-IG samples, we can assume that the electric polarization in Dy-IG is AFE in origin and the corresponding AFE phase has zero total electric polarization.

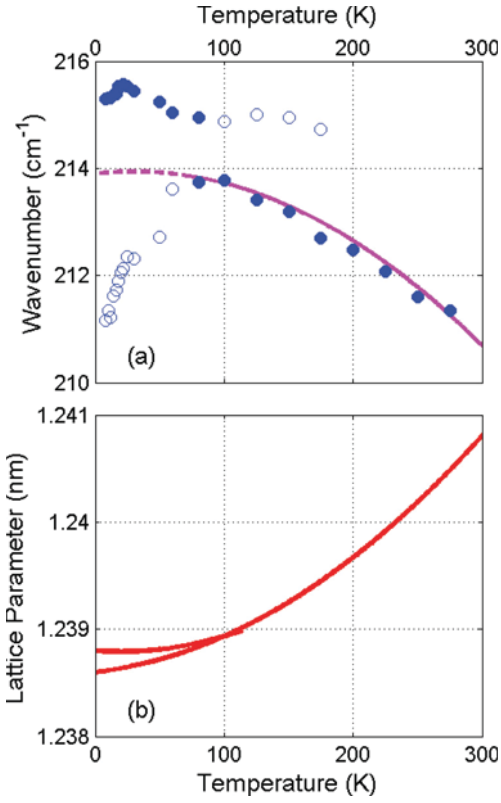

FIG. 12. (Color online) (a) Temperature dependence of the frequency for the E phonon. Note the splitting into two components for $T < 125$ K and the anticrossing at ~70 K. The solid curve is a result of the calculations using Eq. (4). The dashed part of the curve also corresponds to Eq. (4) for the temperature range of the rhombohedral distortion using the average value of the thermal expansion coefficient. (b) Temperature dependence of the lattice parameter for Dy-IG from Ref. 21.

The weak G and K modes are phonons in spite of their relatively weak oscillator strength. On one hand, their oscillator strength is typical for the CF lines, but on the other hand, these peaks are measurable at temperatures up to 300 K, which is more common for phonons and is not expected for the CF transitions due to repopulation of the CF electronic levels at high temperature.

Another weak spectral feature at 442 cm^{-1}, which we observed in the broad temperature range, is not a phonon mode. This spectral anomaly, which we marked LO in Table I, is related to the energy loss in the spectral range where $\varepsilon_1(\omega) \approx 0$. The reason for appearance of this mode is related to the symmetry lowering due to rhombohedral distortion and thus the small dielectric anisotropy between the x, y, and z directions in the measured crystals. We were able to reproduce this spectral feature using our 4×4 Berreman's fitting model by introducing a small anisotropy in ε_∞ and without assigning any additional oscillator to this spectral range.

In the following we will try to relate the temperature-induced peak in $\varepsilon(0,T)$ with the experimentally determined parameters of the phonon spectra. Figure 1(b) shows that the temperature dependence of $\varepsilon(0,T)$ has a major contribution from the combined oscillator strength of all optical modes in the frequency range between 81 and 660 cm^{-1}, which was

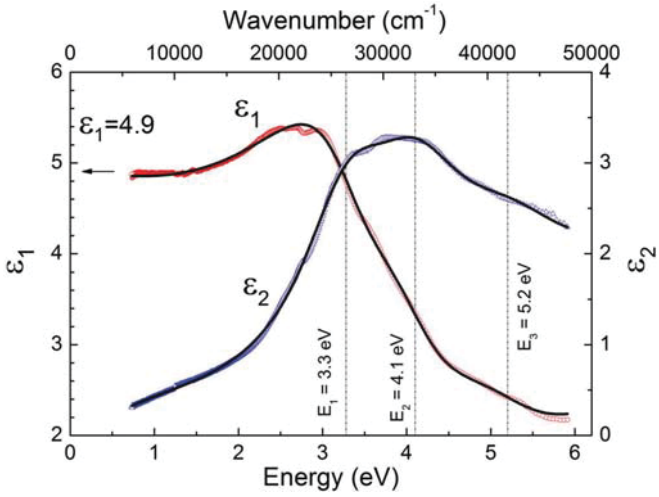

FIG. 13. (Color online) Real and imaginary parts of the dielectric function ε_1 (red circles) and ε_2 (blue triangles) for a Dy-IG measured with AOI = 75° at $T = 300$ K. The extrapolated low-energy value of ε_1 is 4.9. The results of the fit to the dielectric function model that consists of three electronic transitions at 3.3 eV, 4.1 eV, and 5.2 eV and a Penn gap at 7.7 eV (above the measured spectral range) are shown with black solid curves.

determined from the fit of the RAE spectra. The average total oscillator strength of the optical phonons at low temperatures is close to $\sum_j^N S_j \approx 11.2$, which accounts for more than 2/3 of the average static value of the dielectric constant [$\varepsilon(0) \approx 16.5$ in Fig. 1(b)] through the LST relation: $\varepsilon(0) = \varepsilon_\infty + \sum_j^N S_j$. The difference between $\varepsilon(0)$ and $\sum_j^N S_j$ is about 5.3, which is due to the contribution from the high-energy electronic transitions. Unfortunately the accuracy of our ellipsometry measurements above the highest phonon frequency (~700 cm^{-1}) was not high enough and we had to treat ε_∞ as a temperature-independent fitting parameter in the whole temperature range: $\varepsilon_\infty = 5$. To confirm that this value of $\varepsilon_\infty = 5$ is of the right order of magnitude, we carried out additional RAE measurements of the same sample at room temperature in the energy range between 0.75 eV and 5.9 eV. The results of the measurements for the real and imaginary parts of the dielectric function, ε_1 and ε_2 are shown in Fig. 13. The fit to the dielectric function model that consists of three electronic transitions at 3.3 eV, 4.1 eV, and 5.2 eV and a Penn gap at 7.7 eV (above the measured spectral range) is shown with black solid curves. In the low-energy limit, the experimental value of ε_1 is close to 4.9, while ε_2 approaches zero. Thus, we can confirm that the fitting parameter $\varepsilon_\infty = 5$ that have been used for the phonon frequency range is reasonably close to the room temperature value for $\varepsilon(6000\,cm^{-1}) = 4.9$.

Figures 1(b) and 11(b) show a substantial correlation between the small change of the static dielectric constant of $\Delta\varepsilon(0,T) \approx 0.15$ around $T_C = 16$ K and the temperature-dependent oscillator strength the optical phonons. As seen in Fig. 11(b), the temperature anomaly in $\sum_j^N S_j$ is determined primarily by the contribution of the B and C phonons. In spite of this obvious correlation between $\Delta\varepsilon(0,T) \approx 0.15$ and $\sum_j^N S_j(T) \approx 0.2$ for the B and C phonons at $T_C = 16$ K, we cannot completely exclude other possible contributions to the

temperature-induced peak in the static dielectric function, such as from crystal defects and high-energy electronic transitions around and above 4 eV. Additional dc measurements of $\varepsilon(0,T)$ at variable frequencies and UV-ellipsometry experiments at variable temperatures around $T_C = 16$ K could clarify this question.

VII. CONCLUSIONS

The LF and KK exchange excitations have been studied in the far-IR transmission spectra of Dy-IG. Their temperature dependencies allowed us to estimate the ratio between the Fe-Dy and Dy-Dy exchange constants to be $\lambda_{\mathrm{Dy-Dy}}/\lambda_{\mathrm{Fe-Dy}} = 0.13$. The FM phase for Dy-Dy spin interaction was observed for $T < 16$ K and $H < 3.5$ kOe. We show that the combined oscillator strength of the low-frequency KK excitations at 43, 51, and 59.5 cm^{-1} contributes mostly to the static values of magnetic susceptibility $\chi(0,H)$. Since no obvious correlation between the oscillator strength of the KK and LF modes and the magnetic field dependence of the static value of the dielectric constant $\varepsilon(0,H)$ was found, we conclude that the small increase in $\varepsilon(0,H)$ near $H = 1$ kOe is not related to the KK and LF excitations. The oscillator strength of the optical phonons, which were measured using RAE at zero magnetic field, may be related to the temperature variation of the static dielectric constant $\varepsilon(0,T)$ around $T_C = 16$ K. The oscillator strength for the low-frequency optical phonons (marked B and C) at 110 and 113 cm^{-1} is comparable with the peak in $\varepsilon(0,T)$ through the LST relation: $\Delta\varepsilon(0,T) \approx \Delta S_B(T) + \Delta S_C(T)$.

ACKNOWLEDGMENTS

The authors are thankful to G. L. Carr for help at the U4IR beamline. The far-IR transmission experiments at NJIT were supported by NSF under Grant No. DMR-0546985. The crystal growth and magnetic characterization of the samples at Rutgers University were supported by DOE DE-FG02-07ER46382. Use of the National Synchrotron Light Source, Brookhaven National Laboratory, was supported by the US Department of Energy, Office of Science, Office of Basic Energy Sciences, under Contract No. DE-AC02-98CH10886. The far-IR ellipsometry measurements at the University of Fribourg were supported by the LiMAT Fellowship and by SNF grants 200020-129484 and NCCR-MaNEP. The visible ellipsometry measurements have been carried out at the Center for Functional Nanomaterials, Brookhaven National Laboratory, which is supported by the US Department of Energy, Office of Basic Energy Sciences, under Contract No. DE-AC02-98CH10886.

*tdkang@njit.edu

[1] K. P. Belov and V. I. Sokolov, Usp. Fiz. Nauk **121**, 285 (1977) [Sov. Phys. Usp. **20**, 149 (1977)].
[2] N. Hur, S. Park, S. Guha, A. Borissov, V. Kiryukhin, and S.-W. Cheong, Appl. Phys. Lett. **87**, 042901 (2005).
[3] D. Louca, K. Kamazawa, and T. Proffen, Phys. Rev. B **80**, 214406 (2009).
[4] T. D. Kang, E. Standard, K. H. Ahn, A. A. Sirenko, G. L. Carr, S. Park, Y. J. Choi, M. Ramazanoglu, V. Kiryukhin, and S.-W. Cheong, Phys. Rev. B **82**, 014414 (2010).
[5] P. D. Rogers, Y. J. Choi, E. C. Standard, T. D. Kang, K. H. Ahn, A. Dubroka, P. Marsik, C. Wang, C. Bernhard, S. Park, S. W. Cheong, M. Kotelyanskii, and A. A. Sirenko, Phys. Rev. B **83**, 174407 (2011).
[6] N. Hur, S. Park, P. A. Sharma, J. S. Ahn, S. Guha, and S.-W. Cheong, Nature (London) **429**, 392 (2004).
[7] T. Kimura, T. Goto, H. Shintani, K. Ishizaka, T. Arima, and T. Tokura, Nature (London) **426**, 55 (2003).
[8] S.-W. Cheong and M. Mostovoy, Nat. Mater. **6**, 13 (2007).
[9] B. Lorenz, A. P. Litvinchuk, M. M. Gospodinov, and C. W. Chu, Phys. Rev. Lett. **92**, 087204 (2004).
[10] T. Lottermoser and M. Fiebig, Phys. Rev. B **70**, 220407(R) (2004).
[11] A. Pimenov, A. A. Mukhin, V. Yu. Ivanov, V. D. Travkin, A. M. Balbashov, and A. Loidl, Nat. Phys. **2**, 97 (2006).
[12] D. J. Lockwood and M. G. Cottam, J. Appl. Phys. **64**, 5876 (1988).
[13] K. Wakamura and T. Arai, J. Appl. Phys. **63**, 5824 (1988).
[14] A. B. Sushkov, O. Tchernyshyov, W. Ratcliff, S. W. Cheong, and H. D. Drew, Phys. Rev. Lett. **94**, 137202 (2005).
[15] A. B. Sushkov, R. V. Aguilar, S. Park, S.-W. Cheong, and H. D. Drew, Phys. Rev. Lett. **98**, 027202 (2007).
[16] T. Rudolf, Ch. Kant, F. Mayr, and A. Loidl, Phys. Rev. B **77**, 024421 (2008).
[17] Ch. Kant, T. Rudolf, F. Schrettle, F. Mayr, J. Deisenhofer, P. Lunkenheimer, M. V. Eremin, and A. Loidl, Phys. Rev. B **78**, 245103 (2008).
[18] R. Schleck, R. L. Moreira, H. Sakata, and R. P. S. M. Lobo, Phys. Rev. B **82**, 144309 (2010).
[19] R. Schleck, Y. Nahas, R. P. S. M. Lobo, J. Varignon, M. B. Lepetit, C. S. Nelson, and R. L. Moreira, Phys. Rev. B **82**, 054412 (2010).
[20] J. Kaplan and C. Kittel, J. Chem. Phys. **21**, 760 (1953).
[21] F. Sayetat, J. Magn. Magn. Mater. **58**, 334 (1986).
[22] F. Sayetat, J. X. Boucherle, and F. Tcheou, J. Magn. Magn. Mater. **46**, 219 (1984).
[23] R. Hock, H. Fuess, T. Vogt, and M. Bonnet, J. Solid State Chem. **84**, 39 (1990).
[24] M. Lahoubi, M. Guillot, A. Marchand, F. Tcheou, and E. Roudaut, IEEE Trans. Magn. **20**, 1518 (1984).
[25] M. Lahoubi, W. Younsi, M. L. Soltani, J. Voiron, and D. Schmitt, J. Phys.: Conf. Ser. **150**, 042108 (2009).
[26] M. Lahoubi, W. Younsi, M.-L. Soltani, and B. Ouladdiaf, J. Phys.: Conf. Ser. **200**, 082018 (2010).
[27] C. Bernhard, J. Humlíček, and B. Keimer, Thin Solid Films **455-456**, 143 (2004).
[28] A. J. Sievers and M. Tinkham, Phys. Rev. **129**, 1995 (1963).
[29] M. Tinkham, Phys. Rev. **124**, 311 (1961).
[30] J. Yamamoto, B. T. Smith, and E. E. Bell, J. Opt. Soc. Am. **64**, 880 (1974).

[31]G. H. Dieke, *Spectra and Energy Levels of Rare Earth Ions in Crystals* (Wiley, New York, 1968).
[32]P. Grunberg, S. Hufner, E. Orlich, and J. Schmitt, Phys. Rev. **184**, 285 (1969).
[33]P. Grunberg and J. A. Koningsten, J. Opt. Soc. Am. **61**, 1613 (1971).
[34]N. T. McDevitt, J. Opt. Soc. Am. **59**, 1240 (1969).
[35]P. Grunberg and J. A. Koningsten, J. Opt. Soc. Am. **61**, 1613 (1971).
[36]P. D. Rogers, T. D. Kang, T. Zhou, M. Kotelyanskii, and A. A. Sirenko, Thin Solid Films **519**, 2668 (2011).
[37]J. Ménéndez and M. Cardona, Phys. Rev. B **29**, 2051 (1984).